ADVANCED OPTICAL MATERIALS
www.advopticalmat.de

# Coherent-Resonance Enhancement of Sensing at the Exceptional Points

*Jingming Chen, Qinnan Xie, Jingjing Zhang,* Zhuo Li, Tie Jun Cui,* and Yu Luo**

**The branch point singularities in the Riemann surface of the parameter space are known as the exceptional points (EPs), at which two or more eigenvalues and their associated eigenvectors simultaneously coalesce. The abrupt bifurcation property around an EP shows a strong spectral response to external perturbations, and hence, is exploited as a new approach to ultrasensitive sensors. Recently, an intriguing proposal for implementing second-order EPs in optical resonators with external perturbations has shown the superiority of non-Hermitian degeneracies in the enhancement of sensing. Of particular importance is further improving the sensitivity to even greater extents. To this end, a novel physical mechanism is proposed, namely introducing extra resonances of external Rayleigh scatterers to accomplish strong-coupling augmentation in sensing. The results, grounded by both theoretical coupled-mode-theory calculations and experimental spectral-domain measurements, show that the EP-based sensor working at the coherent resonance equips simultaneously substantial perturbation strength and azimuth sensitivity even subjected to extremely weak perturbations. This work paves the way to a new class of highly functional tunable sensors for applications in optics, microwave and acoustics.**

## 1. Introduction

High-quality whispering gallery microcavities such as micro-sphere,[1] micro-toroid,[2] and micro-disk[3] play crucial roles in many applications involving the detection/sensing of small perturbations[4–10] and/or measurement of weak signals.[10,11] An ideal azimuthally symmetric resonator supports two counter-propagating whispering gallery modes (WGMs), i.e., clockwise (CW) and counter-clockwise (CCW) ones at the diabolic point (DP) with a degenerate eigenfrequency but non-degenerate eigenstates. When a DP-based sensor is perturbated by surface defects or external scatterers, backscattering triggers modal coupling between CW and CCW travelling waves, giving rise to frequency splitting that is linearly proportional to the perturbation strength. Although some DP-based sensors with ultrahigh Q-factor have been applied to the weak measurement such as the single nanoparticle/molecule detection, their linear response characteristics render them ineffective against extremely weak perturbations. Recently, an innovative type of sensor, known as the exceptional point (EP) sensor, is proposed to overcome this drawback.[12–16] Unlike traditional DP-based sensors, a sensor operating in the vicinity of a N-th-order EP exhibits a N-th-root frequency response to the perturbation strength. In other words, for a sufficiently small perturbation, the frequency splitting is parametrically larger, i.e., a unique characteristic resulting from non-Hermitian degeneracies.

Exceptional point is the hallmark of non-Hermitian systems and has been extensively explored in a variety of parity-time

J. Chen, Q. Xie, J. Zhang, T. J. Cui
Institute of Electromagnetic Space
Southeast University
Nanjing 210096, China
E-mail: zhangjingjing@seu.edu.cn; tjcui@seu.edu.cn

J. Chen, Q. Xie, J. Zhang, T. J. Cui
State Key Laboratory of Millimeter Waves
Southeast University
Nanjing 210096, China

J. Chen
Department of Electrical and Electronic Engineering
Southern University of Science and Technology
Shenzhen 518055, China

Q. Xie, J. Zhang, T. J. Cui
Frontiers Science Center for Mobile Information Communication and Security
Southeast University
Nanjing 210096, China

Z. Li, Y. Luo
Key Laboratory of Radar Imaging and Microwave Photonics
Ministry of Education
College of Electronic and Information Engineering
Nanjing University of Aeronautics and Astronautics
Nanjing 211106, China
E-mail: yu.luo@nuaa.edu.cn

Y. Luo
School of Electrical and Electronic Engineering
Nanyang Technological University
Nanyang Avenue 639798, Singapore

The ORCID identification number(s) for the author(s) of this article can be found under https://doi.org/10.1002/adom.202302268

**DOI: 10.1002/adom.202302268**

 

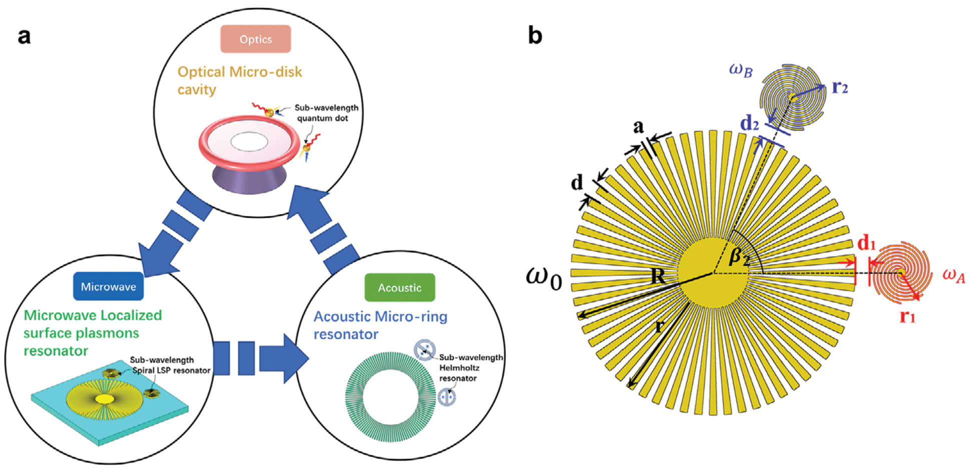


**Figure 1.** The schematic diagrams of coherent-resonance enhanced EP-based sensors. a) Coherent-resonance enhanced EP-based sensors in optical, microwave and acoustic wave regimes via perturbing the WGM with two external subwavelength resonators that resonant coherently with the WGM. b) A coherent-resonance enhanced EP-based sensor consisting of an azimuthally symmetric spoof LSP resonator (with $R = 12$ mm, $r = 9$ mm, $d = 1.255$ mm, $a = 0.625$ mm) and two subwavelength spiral-shaped spoof LSP resonators (with $r_1 = 2.6$ mm, $r_2 = 2.8$ mm, respectively).

(PT)-symmetric systems with balanced gain and loss.[17–24] The typical example is a coupled cavity/waveguide system with a judiciously tailored gain–loss distribution.[17–24] The non-Hermicity can also be manipulated in all-passive systems through the control of the resonator geometry. Based on this scheme, the EP is achieved in shape-deformed microcavities,[25–27] chiral resonators array,[16] multilayered plasmonic nanoantenna arrays[28] and microcavities scattered by external nanotips.[12–14]

The setup we worked on is motivated by one intriguing proposal for EP-based sensors, i.e., whispering gallery microcavity with two external Rayleigh scatterers.[12–14] In previous work, this strategy has been implemented at optical frequencies and nearly twofold sensitivity enhancement was observed.[14] To further enhance the sensitivity, one can either implement a higher-order non-Hermitian degeneracy (i.e., increase the root order of the frequency response to the perturbation strength) or push the coupling strength between the microcavity and Rayleigh scatterers to the strong-coupling regime. Since small perturbations are generally accompanied with weak coupling, previous approaches make use of higher-order EPs to achieve higher-order non-Hermitian degeneracies, so as to enhance the sensitivity.[15,16] However, higher-order EPs are often implemented with multiple microcavities and generally require precise control of the gain/loss or backscattering of each resonator,[15,16] where the implementation is very complex and the system is unstable. In this paper, we propose a different scheme to enhance EP sensing, through the introduction of coherent resonances to the external Rayleigh scatterers. Based on the coupled mode theory, we show that the resonant frequency of the Rayleigh scatterer provides an extra degree of freedom to effectively control the coupling strength between the microcavity and external Rayleigh scatterers. The sensitivity of the system is maximized when the external Rayleigh scatterers resonate coherently with the WGMs. As an experimental proof, we implement the deep-subwavelength scatterers based on spoof localized surface plasmons and observe over one order of magnitude sensitivity enhancement in a single whispering gallery microcavity without increasing the order of EP. Finally, we stress that the strategy proposed in this work is fairly general and can be easily extended to optical frequencies and even to other wave systems such as acoustics, as depicted in **Figure 1**a.

## 2. Results and Discussion

The specific structures we propose and investigate consist of one spoof localized surface plasmons (LSP) resonator[29,30] and two nonidentical sub-wavelength spiral-shaped spoof LSP resonators[31–34] as illustrated in Figure 1b. Here, we fix the position of one spiral-shaped LSP resonator (marked in red, azimuthal position $\beta_1 = 0$, distance $d_1 = 0.5mm$) and precisely tailor the relative position of the second spiral-shaped LSP resonator (marked in blue). The complex frequency splitting tends to vanish at some particular positions when the two sub-wavelength resonators induce fully asymmetric backscattering between CW and CCW travelling waves.

Here, we employ a theoretical model with two-mode approximation to describe this system. The effective $2 \times 2$ Hamiltonian in CW and CCW travelling waves basis is:

$$H_{EP} = \begin{pmatrix} \omega^{(2)} & A^{(2)} \\ B^{(2)} & \omega^{(2)} \end{pmatrix} \tag{1}$$

with

$$\omega^{(2)} = \omega_0 + \epsilon_1 + \epsilon_2$$
$$A^{(2)} = \epsilon_1 e^{-i2m\beta_1} + \epsilon_2 e^{-i2m\beta_2}$$
$$B^{(2)} = \epsilon_1 e^{+i2m\beta_1} + \epsilon_2 e^{+i2m\beta_2} \tag{2}$$

where $\omega_0$ is the complex resonant frequency of unperturbed CW (or CCW) travelling waves; $m$ is the azimuthal mode number of the WGMs; $\epsilon_1$ ($\epsilon_2$) is the half of the complex frequency splitting when the WGMs is perturbed by the spiral-shaped resonator1 (2) alone; $\beta_1$ ($\beta_2$) is the angular position of spiral-shaped resonator1

(2) (we set $\beta_1 = 0$ throughout the manuscript). Note that $\omega_0$, $\epsilon_1$, and $\epsilon_2$ are set to complex numbers to take into account the loss effect (i.e., scattering and/or dissipation). $A^{(2)}$ ($B^{(2)}$) quantify the amount of backscattering from CW (CCW) to CCW (CW) travelling wave. Particularly, in the case of the fully asymmetric backscattering between CW and CCW travelling waves, e.g., $A^{(2)} \neq 0$ and $B^{(2)} = 0$, two WGMs coalesce at the exceptional point.

When a target scatterer enters into the evanescent field region to disturb the DP (EP)-based sensor, the resonance of the system will deviate from the DP (EP), thereby lifting the degeneracy of eigenmodes and triggering the complex frequency splitting. According to the perturbation theory, the system Hamiltonian in the presence of the perturbation can be written as $H_{1(2)} = H_{DP(EP)} + H_0$, where $H_{DP(EP)}$ is the system Hamiltonian without the perturbation and $H_0$ corresponds to the deviation caused by the perturbation. For example, the DP-based sensor subject to a perturbation $\epsilon_0$ is described by the following Hamiltonian:

$$H_1 = H_{DP} + H_0 = \begin{pmatrix} \omega_0 & 0 \\ 0 & \omega_0 \end{pmatrix} + \begin{pmatrix} \epsilon_0 & \epsilon_0 e^{-i2m\beta_0} \\ \epsilon_0 e^{+i2m\beta_0} & \epsilon_0 \end{pmatrix} \tag{3}$$

where $\beta_0$ is the angular position of the target scatterer. Since the complex frequency splitting $\Delta\omega_{DP}$ is the difference of the two eigenvalues of $H_1$, Equation 3 gives $\Delta\,\omega_{DP} = 2\epsilon_0$, implying that $\Delta\omega_{DP}$ is linearly proportional to the perturbation $\epsilon_0$. In the case of EP-based sensors, previous works[12–14] show that the system Hamiltonian takes the form of:

$$H_2 = H_{EP} + H_0 = \begin{pmatrix} \omega^{(2)} & A^{(2)} \\ 0 & \omega^{(2)} \end{pmatrix} + \begin{pmatrix} \epsilon_0 & \epsilon_0 e^{-i2m\beta_0} \\ \epsilon_0 e^{+i2m\beta_0} & \epsilon_0 \end{pmatrix} \tag{4}$$

where the eigenvalue difference (and hence the frequency splitting $\Delta\omega_{\mathrm{EP}}$) is proportional to $\sqrt{\epsilon_0}$.[12–14] This quadratic relationship significantly enhances the frequency splitting at small $\epsilon_0$. We highlight that Equation 4 is valid only when the two Rayleigh scatterers introduced to the EP sensor do not resonate with the WGMs. When the two Rayleigh scatterers and the WGMs resonate coherently with each other, in this case, the Hamiltonian of the EP sensor should be modified according to $H_2 = H_{EP} + \boldsymbol{\alpha} H_0$ (see Supplementary Materials S2, Supporting Information). Note that an enhancement factor $\alpha$ is introduced because the relatively strong coupling[35,36] between the resonant Rayleigh scatters and the whispering gallery microcavity significantly modifies the perturbation strength $\epsilon_0$, leading to enhanced frequency splitting deduced as:

$$\frac{\Delta\omega_{EP}}{\Delta\omega_{DP}} = \alpha\sqrt{1 + \frac{A^{(2)}}{\alpha\epsilon_0} e^{i2m\beta_0}} \tag{5}$$

In other words, the resonance of the Rayleigh scatter introduces another degree of freedom to engineer the spectral responses of the EP-based sensor.

Equation 5 indicates that the frequency splitting of the EP-based sensor is significantly larger than that of the DP-based one because of two factors: 1) the enhancement factor $\alpha$ resulting from the resonance of the Rayleigh scatter; 2) $\sqrt{1 + \frac{A^{(2)} e^{i2m\beta_0}}{(\alpha\epsilon_0)}}$ corresponding to the non-Hermitian degeneracy at the EP. When $\alpha \to 1$, Equation 5 reduces to the case of traditional EP-based sensors,[12–14] where the sensitivity enhancement is dominant by the non-Hermitian degeneracy. On the other hand, when $\alpha > 1$, $|\Delta\omega_{EP}/\Delta\omega_{DP}|$ is positively correlated with both the enhancement factor $\alpha$ and the backscattering coefficient $|A^{(2)}|$, giving rise to further sensitivity enhancement as $\alpha$ increases.

Equation 5 also offers us the stepping stone to explore other exotic phenomena such as higher azimuth sensitivity by engineering the enhancement factor $\alpha$. We highlight that $\alpha$ can be effectively controlled by tuning the resonance of the sub-wavelength spiral-shaped resonator. To illustrate this point, we select the sixth-order WGMs ($m = 6$) at $\omega_0 = 9.8048$ GHz as the characteristic modes and design dipolar modes of two spiral-shaped resonators with $\omega_A = \omega_B = \eta \times \omega_0$ by tuning the structural parameters, where $\eta$ is the degree of the resonance coherence. We consider three different EP-based sensors with $\eta = \infty$ (fully noncoherent), $\eta = 1.05\omega_0$ (partially coherent), $\eta = \omega_0$ (fully coherent), respectively. The corresponding geometries of the three structures are plotted in **Figure** 2a–c. For simplicity, we first consider the 2D scenario, where the structure is infinite along the axial direction. The complex eigenvalues and eigenstates of the system around the corresponding EPs are numerically computed with COMSOL Multiphysics. The real and imaginary parts of eigenfrequencies exhibit a square root dependence on the relative angular position $\beta_2 - \beta_1$ near the branch points, i.e., EPs (see Figure 2d,f,h). The eigenmode field distributions ($|H_z|^2$) (see Figure 2e,g,i) of the paired modes show the same chirality, proving that these systems operate at EPs. More interestingly, we find that the fully coherent EP-based sensor exhibits the largest mode splitting (corresponding to the highest sensitivity) when deviating from EPs.

In order to verify our theoretical model and ascertain the dependence of the sensitivity enhancement on the degree of the resonance coherence, we conduct further simulations by introducing a circular dielectric particle (refractive index 1.5, radius 0.5 mm) at the angular position $\beta_0 = \pi$ as the target scatterer. The logarithmic plot of the absolute frequency splitting $|\Delta\omega|$ in terms of the perturbation strength $\epsilon_0$ is plotted in **Figure** 3a, where the target scatterer is located in the vicinity of a DP-based sensor (black point) and five different EP-based sensors (colored points) labeled by the degree of the resonance coherence $\eta = \infty, 1.05\omega_0, 1.03\omega_0, 1.01\omega_0, \omega_0$ respectively. The DP-based sensor exhibits a linear relationship with a slope of 1, confirming the linear response to the perturbation strength around the diabolic point, whereas the EP-based sensor exhibits a slope of 1/2, indicating that perturbations around the exceptional point experience an enhancement in the terms of $\epsilon^{1/2}$.

Figure 3b displays the sensitivity enhancement $|\Delta\omega_{EP}/\Delta\omega_{DP}|$ of the five EP-based sensors as a function of the perturbation strength $\epsilon_0$. The colored solid curves are fitted with Equation 5, showing remarkable quantitative agreement between the simulation and the theoretical formula. Apparently, the sensitivity of the system increases dramatically as $\eta$ approaches 1. The inset in Figure 3b confirms that the fitted enhancement factor $\alpha$ increases exponentially with decreasing $\eta$, consistent with the predictions of Equation 5: the sensitivity of EP-based sensors can be significantly improved by tuning the degree of resonance coherence between the WGMs and the spiral-shape resonators.

 

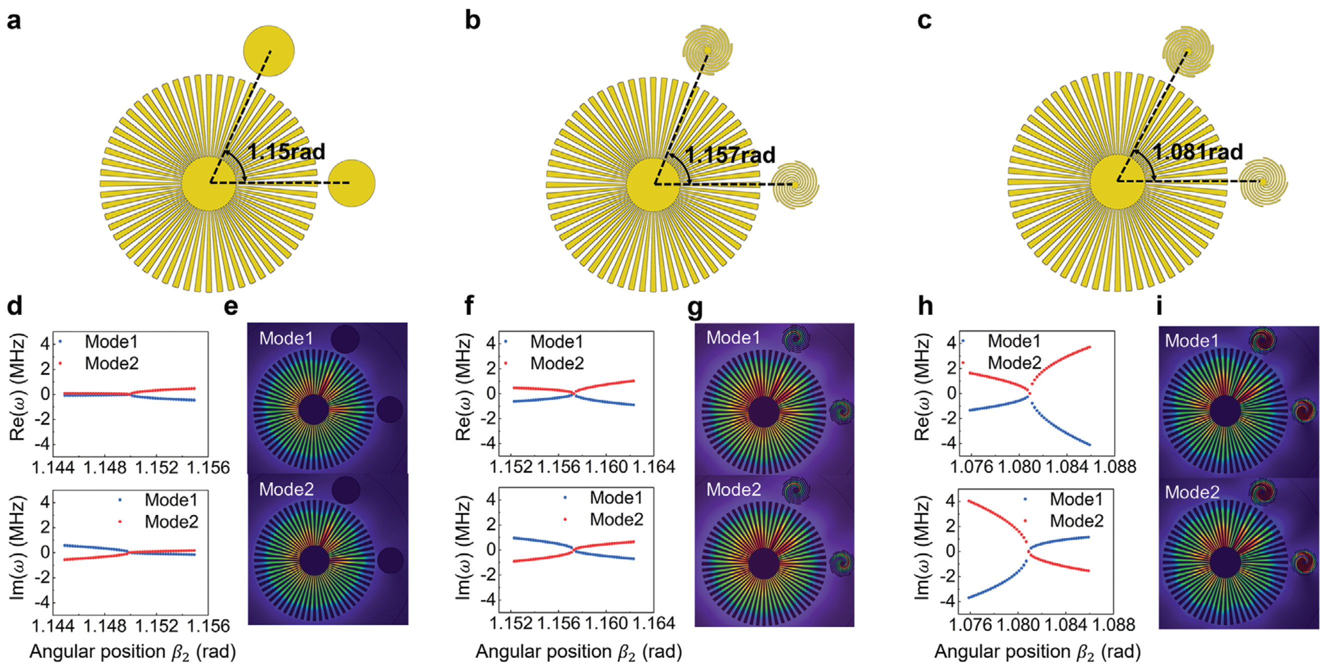


**Figure 2.** Eigenvalues and eigenfields near the exceptional points generated from different resonance coherences. a–c) Schematic diagrams of three different exceptional-point sensors, where the resonant frequencies of external spiral-shaped resonators are ∞ (fully noncoherent) (a), $1.05\omega_0$ (partially coherent) (b), $\omega_0$ (fully coherent) (c), respectively. d,f,h) The real and imaginary parts of eigenfrequencies for three systems near homologous EPs as functions of the relative angular position $\beta_2$. e,g,i) The corresponding fields distributions ($|H_z|^2$) of paired EPs eigenmodes.

Larger enhancement factor $\alpha$ not only improves the sensitivity, but also provides a possible route to detect the azimuth position of the perturbation, even under extremely small perturbation strength. We highlight that high azimuthal sensitivity is difficult to realize with both conventional DP- and EP-based sensors. To demonstrate this point, we first consider the conventional EP-based sensor out of the coherent resonance where $\alpha \rightarrow 1$. For sufficiently small perturbations $\epsilon_0 \ll 1$, the sensitivity enhancement is calculated as:

$$\frac{\Delta\omega_{EP}}{\Delta\omega_{DP}} = \sqrt{\frac{A^{(2)}}{\alpha\epsilon_0}}e^{im\beta_0} \tag{6}$$

Equation 6 indicates that the real and imaginary parts of $\Delta\omega_{EP}/\Delta\omega_{DP}$ are periodic functions of $\beta_0$, whereas the corresponding absolute value remains a constant. Such a behavior is confirmed by **Figure 4a** that shows that the simulated real (imaginary) part of the complex sensitivity enhancement changes

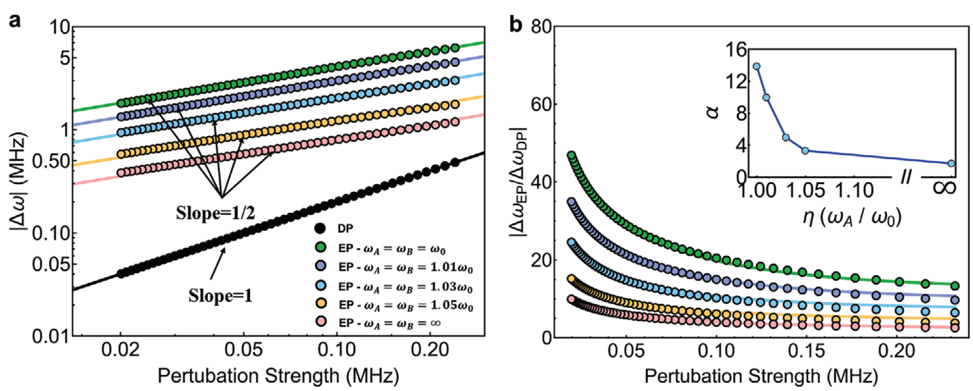


**Figure 3.** Dependence of sensitivity enhancement of EP-based sensors on the degree of resonance coherence. a) Logarithmic plot of the absolute frequency splitting $|\Delta\omega|$ versus the perturbation strength $\epsilon_0$, when a target dielectric particle is moved toward a DP-based sensor (black point) and five EP-based sensors (colored points) involving subwavelength resonators with different degrees of resonance coherence, ∞, $1.05\omega_0$, $1.03\omega_0$, $1.01\omega_0$, $\omega_0$, respectively. The DP-based sensor exhibits a linear relationship with the slope of 1, whereas the EP-based sensors exhibit a slope of 1/2, confirming the square root topology of second order exceptional points. b) The sensitivity enhancements $|\Delta\omega_{EP}/\Delta\omega_{DP}|$ for five EP-based sensors as functions of the perturbation strength $\epsilon_0$. The colored solid curves are fitted with theoretical formula Equation 5. The inset displays the decay relationships between fitted $\alpha$ and the degree of resonance coherence $\eta$.

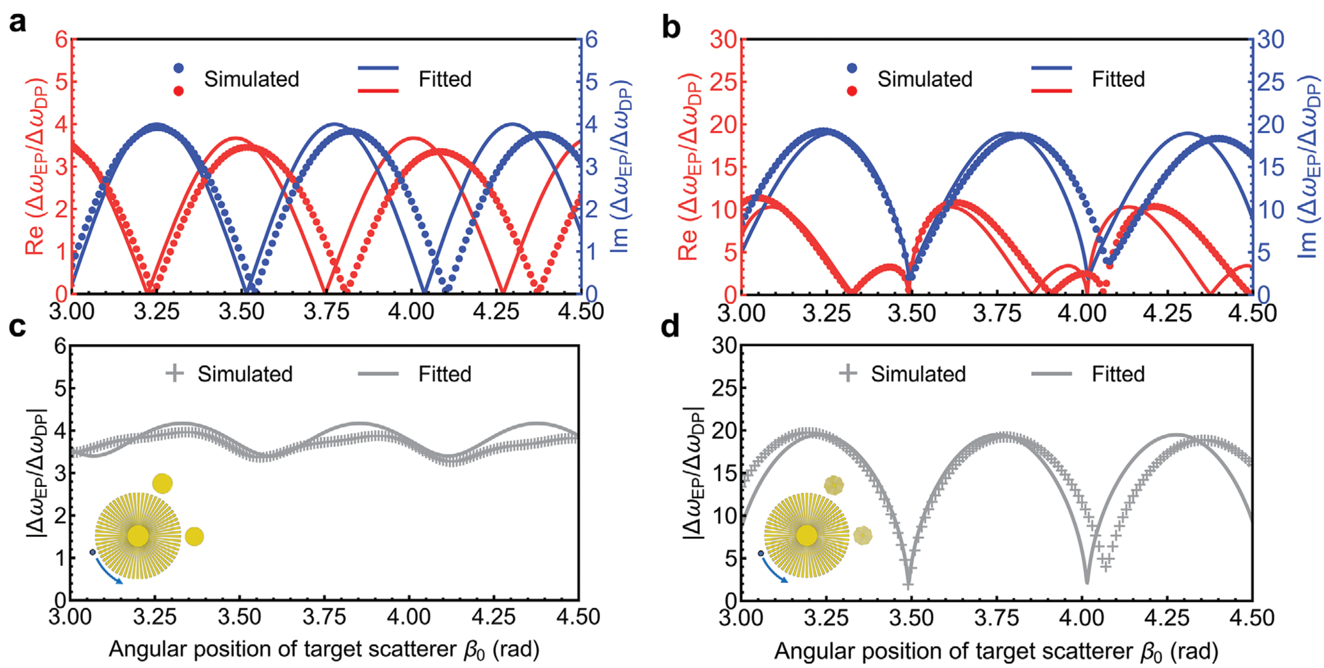


**Figure 4.** The sensitivity enhancement as a function of the angular position of the target scatterer with sufficiently modest perturbation strength. a,c) The real and imaginary part (a) and the absolute value (c) of the complex sensitivity enhancement as a function of the angular position of the target scatterer, for a conventional EP-based sensor out of coherent resonance. b,d) The real and imagine part (b) and the absolute value (d) of the complex sensitivity enhancement in terms of the angular position of the target scatterer, for a fully coherent resonance EP-based sensor. In both cases, the target scatterer is set 2 mm away from the WGM resonator with its angular position $\beta_0$ varying from 3 to 4.5 radians.

periodically in a cosinoidal (sinusoidal) trend in response to the variation of the angular position of the target scatterer. Accordingly, the absolute value of sensitivity enhancement is approximately a constant ≈3.8 irrespective of $\beta_0$, as shown in Figure 4c. The constant $|\Delta\omega_{EP}/\Delta\omega_{DP}|$ as confirmed by both the theory and simulation reveals that the EP-based sensor out of the coherent resonance exhibits a relatively low azimuthal sensitivity.

In contrast, the EP-based sensor working at the coherent resonance exhibits a completely different behavior, as shown in Figure 4b,d. To make a fair comparison with the conventional EP sensor discussed above, we set the target scatterer at the same position as in Figure 4a,c to introduce the same perturbation strength $\epsilon_0$. We highlight that, because of the large enhancement factor $\alpha$ introduced by the coherent resonance, $\alpha\epsilon_0$ is no longer negligible even if $\epsilon_0 \ll 1$. In this case, the complex sensitivity enhancement $\Delta\omega_{EP}/\Delta\omega_{DP}$ must strictly follow Equation 5 with its real and imaginary parts deviating significantly from the trigonometric trend (See Figure 4b). Remarkably, the absolute value of $\Delta\omega_{EP}/\Delta\omega_{DP}$ also varies dramatically with the angular position $\beta_0$, as confirmed by the simulation in Figure 4d. Such a behavior can be interpreted as the angle-dependent interference between the backscattering induced by the target scatterer and the two LSP resonators when $\alpha\epsilon_0$ is comparable to $A^{(2)}$. In Figure 4, dot lines correspond to simulated data obtained with COMSOL Multiphysics while the solid lines are calculated theoretically using Equation 5. The quantitative agreement demonstrates the validity of our theoretical model. The strong angle-dependent sensitivity enhancement further reveals that fully coherent resonance EP-based sensors have an excellent azimuthal resolution even under extremely weak perturbations

Finally, we proceed to the experimental demonstration, where the DP-based sensor and EP-based sensors with and without coherent resonance are fabricated using the standard printed circuit board fabrication with 18μ*m* thick copper on a 1.575 mm thick RT5880 (permittivity $\epsilon = 2.2 \pm 0.02$, loss tangent $\Delta\delta = 0.0009$) dielectric substrate, as depicted in **Figure 5**a–c. An SSPP waveguide connected to the vector network analyzer is designed to excite the LSP resonances through nearfield coupling. The exceptional points of the EP-based sensors are confirmed by the zero mode-splittings in the transmission spectra, i.e., only a single resonance dip is observed in Figure 5b,c. The non-Hermitian nature of the EP-based sensors is also demonstrated by the measured asymmetric reflection spectra as shown in the insets of the bottom panels of Figure 5b,c.

In order to compare the sensitivities of the three sensing systems above, we introduce a copper particle as the target scatterer into the near-field region of the WGM resonator. The target scatter perturbs the evanescent field of the WGM resonator, resulting in mode splitting in the transmission spectrum, as shown in Figure 5d–f. The sensitivities of the three systems are compared by measuring the mode splitting. Remarkably, the EP-based sensor working at the coherent resonance shows a nearly twofold sensitivity enhancement over that of the conventional EP-based sensor out of the coherent resonance, corresponding to a nearly three-fold sensitivity enhancement over that of the DP-based sensor. Furthermore, in order to demonstrate the dependence of sensitivity enhancement of these two EP-based sensors on the perturbation strength, we proceed to change the size of the copper particle for the three sensors and measure corresponding mode splitting. As shown in **Figure 6**a, the DP-based

 

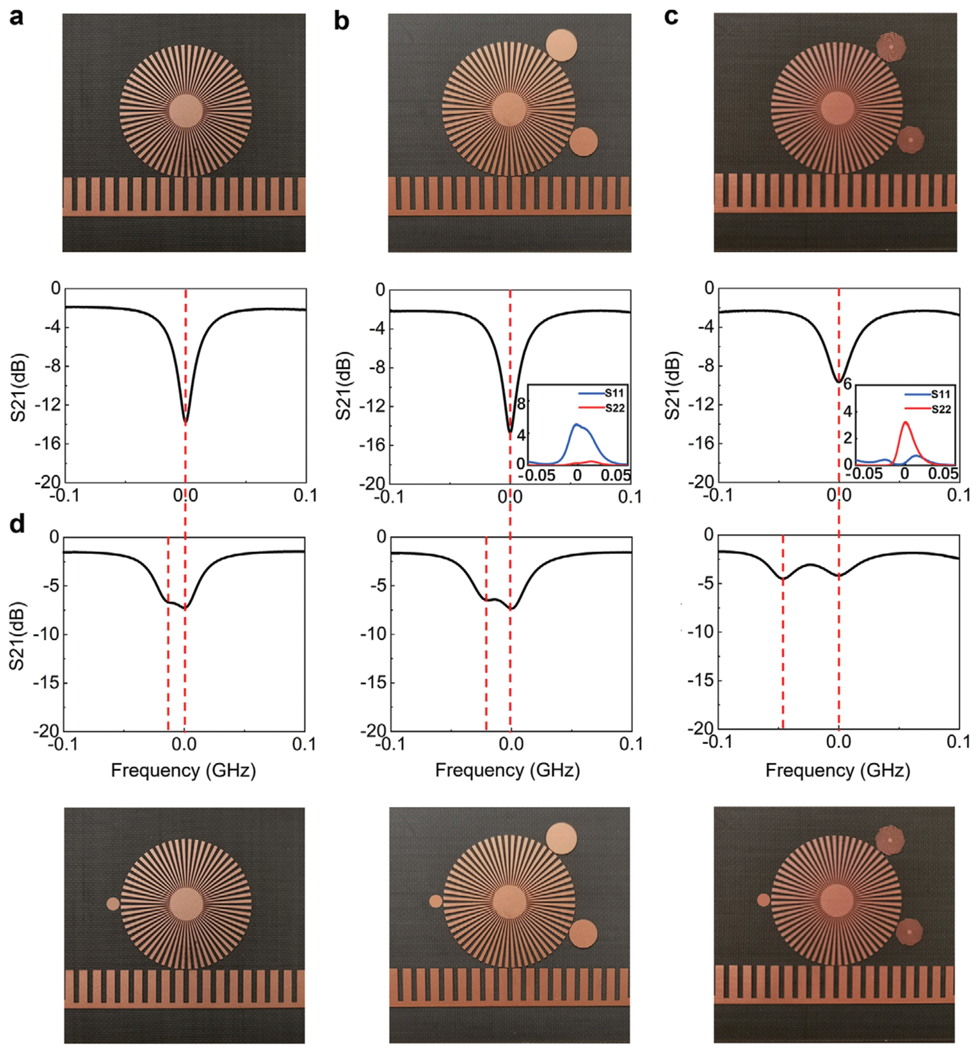


**Figure 5.** Experimental observations on the sensing abilities of the fully noncoherent resonance and fully coherent resonance EP-based sensors. a,d) The transmission spectra of DP-based sensor before (a) and after (d) being perturbated by the copper target scatterer in close proximity to the LSP resonator. b,e) The transmission spectra of fully noncoherent resonance EP-based sensor before (b) and after (e) being perturbated by same copper target scatterer. c,f) The transmission spectra of fully coherent resonance EP-based sensor before (c) and after (f) being perturbated by the same copper target scatterer. The insets in (b) and (c) show the fully asymmetric backscattering with S12 and S21. The red vertical dotted lines highlight the mode splitting and the contrast in sensitivity enhancement is clearly visible.

sensor exhibits a linear relationship with a slope of 1, whereas the EP-based sensors exhibit slopes of 1/2, confirming the linear and square-root response to the perturbation strength around the diabolic point and exceptional point, respectively. Besides, as demonstrated in Figure 6b, the sensitivity enhancement of fully coherent resonance EP-based sensor is nearly two-fold over that of the non-coherent resonance EP-based sensor at a broad perturbation strength region. These measurements successfully validate our aforementioned theoretical model and reveals application prospects of our proposal in sensing enhancement. Note that although the classical (i.e., technical) noise may influence the sensing performance of our proposed EP-based sensors working in the classical wave regime, this type of noise can be reduced, i.e., the signal-to-noise ratio can be increased, by using active device such as low-noise amplifiers and low-pass filters[37] or introducing nonlinear saturable gain.[38]

Detailed discussions on the experiments, including the experimental setup and the design of the systems are provided in Supplementary Materials S3–S6 (Supporting Information).

## 3. Conclusion

In summary, we have proposed a new class of EP-based sensor by introducing coherent resonance between the whispering gallery microcavity and two external sub-wavelength resonators. On the platform of LSP resonators, we have demonstrated theoretically and experimentally that such a fully coherent resonance EP-based sensor exhibits remarkable enhancement of sensitivity over the corresponding fully noncoherent EP-based sensor, providing not only excellent perturbation strength sensitivity, but also azimuth sensitivity even with extremely small perturbations. Our proposed ultrathin EP-based sensor with high sensitivity as

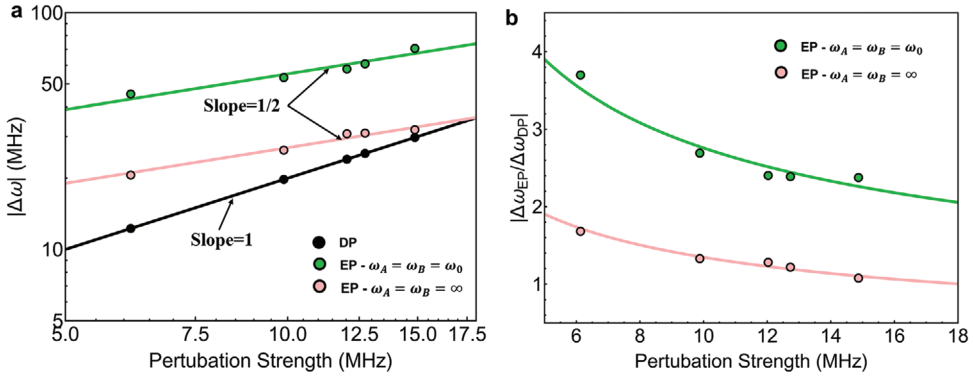


**Figure 6.** Experimental demonstrations on the dependence of sensitivity enhancements of the fully noncoherent resonance and fully coherent resonance EP-based sensors on the perturbation strength. a) Logarithmic plot of the absolute frequency splitting $|\Delta\omega|$ versus the perturbation strength $\epsilon_0$ (changing the size of target copper particle) for a DP-based sensor (black point), fully noncoherent resonance and fully coherent resonance EP-based sensors, respectively. The DP-based sensor exhibits a linear relationship with the slope of 1, whereas the EP-based sensors exhibit a slope of 1/2, confirming the square root topology of second order exceptional points. b) The sensitivity enhancements $|\Delta\omega_{EP}/\Delta\omega_{DP}|$ for two EP-based sensors as functions of the perturbation strength $\epsilon_0$.

well as high angular resolution, may find a broad range of applications in integrated detection and characterization systems. Furthermore, this strategy is fairly general and can be easily extended to other classical wave systems such as optics, acoustics and mechanical wave.

## Supporting Information

Supporting Information is available from the Wiley Online Library or from the author.

## Acknowledgements

J.C. and Q.X. contributed equally to this work. Funding: This work was supported in part by the National key R & D Program of China under Grant no. 2022YFA1404903, the National Science Foundation of China under Grant nos. 62271139, U21A20459, 61871127, 62288101. Y.L was sponsored by National Research Foundation Singapore Competitive Research Program under Grant no. NRF-CRP23-2019-0007. Z. L. was sponsored by the Fund of Qing Lan Project of Jiangsu Province under Grant no. 1004-YQR22031, and the Fund of Prospective Layout of Scientific Research for Nanjing University of Aeronautics and Astronautics under 1004-ILA22002 and 1004-ILA22068.

## Conflict of Interest

The authors declare no conflict of interest.

## Data Availability Statement

The data that support the findings of this study are available from the corresponding author upon reasonable request.

## Keywords

exceptional point, non-Hermitian, optical sensing, spoof plasmonics

Received: September 14, 2023
Revised: January 6, 2024
Published online:

[1] S. M. Spillane, T. J. Kippenberg, K. J. Vahala, *Nature* **2002**, *415*, 621.
[2] D. K. Armani, T. J. Kippenberg, S. M. Spillane, K. J. Vahala, *Nature* **2022**, *421*, 925.
[3] H. Lee, T. Chen, J. Li, K. Y. Yang, S. Jeon, O. Painter, K. J. Vahala, *Nat. Photonics* **2012**, *6*, 369.
[4] A. M. Armani, R. P. Kulkarni, S. E. Fraser, R. C. Flagan, K. J. Vahala, *Science* **2007**, *317*, 783.
[5] F. Vollmer, S. Arnold, D. Keng, *Proc. Natl Acad. Sci., USA* **2008**, *105*, 20701.
[6] L. Shao, X. Jiang, X. Yu, B. Li, W. R. Clements, F. Vollmer, W. Wang, Y. Xiao, Q. Gong, *Adv. Mater.* **2013**, *25*, 5616.
[7] L. He, S. K. Özdemir, J. Zhu, W. Kim, L. Yang, *Nat. Nanotechnol* **2011**, *6*, 428.
[8] F. Vollmer, S. Arnold, *Nat. Methods* **2008**, *5*, 591.
[9] F. Vollmer, L. Yang, *Nanophotonics* **2012**, *1*, 267.
[10] J. Zhu, S. K. Özdemir, Y. Xiao, L. Li, L. He, D. Chen, L. Yang, *Nat. Photonics* **2010**, *4*, 46.
[11] W. Kim, S. K. Özdemir, J. Zhu, M. Faraz, C. Coban, L. Yang, *Opt. Express* **2012**, *20*, 29426.
[12] B. Peng, S. K. Özdemir, M. Liertzer, W. Chen, J. Kramer, H. Yilmaz, J. Wiersig, S. Rotter, L. Yang, *Proc. Natl Acad. Sci., USA* **2016**, *112*, 203901.
[13] J. Wiersig, *Phys. Rev. Lett.* **2014**, *112*, 203901.
[14] W. Chen, S. K. Özdemir, G. Zhao, J. Wiersig, L. Yang, *Nature* **2017**, *548*, 192.
[15] H. Hodaei, A. U. Hassan, S. Wittek, H. Garcia-Gracia, R. El-Ganainy, D. N. Christodoulides, M. Khajavikhan, *Nature* **2017**, *548*, 187.
[16] S. Wang, B. Hou, W. Lu, Y. Chen, Z. Q. Zhang, C. T. Chan, *Nat. Commun.* **2019**, *10*, 832.
[17] C. M. Bender, S. Boettcher, *Phys. Rev. Lett.* **1998**, *80*, 5243.
[18] S. Klaiman, U. Günther, N. Moiseyev, *Phys. Rev. Lett.* **2008**, *101*, 080402.
[19] C. E. Rüter, K. G. Makris, R. El-Ganainy, D. N. Christodoulides, M. Segev, D. Kip, *Nat. Phys.* **2010**, *6*, 192.
[20] B. Peng, S. K. Özdemir, F. Lei, F. Monifi, M. Gianfreda, G. L. Long, S. Fan, F. Nori, C. Bender, L. Yang, *Nat. Phys.* **2014**, *10*, 394.
[21] Y. Sun, W. Tan, H. Q. Li, J. Li, H. Chen, *Phys. Rev. Lett.* **2014**, *112*, 143903.
[22] L. Feng, Z. J. Wong, R. M. Ma, Y. Wang, X. Zhang, *Science* **2014**, *346*, 972.
[23] W. Song, W. Sun, C. Chen, Q. Song, S. Xiao, S. Zhu, T. Li, *Phys. Rev. Lett.* **2019**, *123*, 165701.

 

[24] W. Tang, X. Jiang, K. Ding, Y. X. Xiao, Z. Q. Zhang, C. T. Chan, G. Ma, *Science* **2020**, *370*, 1077.
[25] J. Wiersig, S. W. Kim, M. Hentschel, *Phys. Rev. A* **2008**, *78*, 053809.
[26] J. Wiersig, A. Eberspacher, J. B. Shim, J. W. Ryu, S. Shinohara, M. Hentschel, H. Schomerus, *Phys. Rev. A* **2011**, *84*, 023845.
[27] W. Yan, P. Lalanne, M. Qiu, *Phys. Rev. Lett.* **2020**, *16*, 462.
[28] J. H. Park, A. Ndao, W. Cai, L. Hsu, A. Kodigala, T. Lepetit, Y. H. Lo, B. Kanté, *Nat. Phys.* **2020**, *16*, 462.
[29] X. Shen, T. J. Cui, *Laser Photonics Rev.* **2014**, *8*, 137.
[30] Z. Gao, F. Gao, Y. Zhang, H. Xu, Y. Luo, B. Zhang, *Adv. Mater.* **2018**, *30*, 1700018.
[31] P. A. Huidobro, X. Shen, J. Cuerda, E. Moreno, L. Martin-Moreno, F. J. Garcia-Vidal, T. J. Cui, J. B. Pendry, *Phys. Rev. X* **2014**, *4*, 021003.
[32] Z. Liao, A. I. Fernandez-Dominguez, J. Zhang, S. A. Maier, T. J. Cui, Y. Luo, *ACS Photonics* **2016**, *3*, 1768.
[33] Z. Liao, A. I. Fernandez-Dominguez, X. Shen, S. A. Maier, T. J. Cui, *Sci. Rep.* **2015**, *5*, 9590.
[34] J. Zhang, Z. Liao, Y. Luo, X. Shen, S. A. Maier, T. J. Cui, *Laser Photonics Rev.* **2017**, *11*, 1600191.
[35] N. Kongsuwan, X. Xiao, P. Bai, J. B. You, C. E. Png, L. Wu, O. Hess, *Nano Lett.* **2019**, *19*, 5853.
[36] J. Feist, F. J. Garcia-Vidal, *Phys. Rev. Lett.* **2015**, *114*, 196402.
[37] Z. Xiao, H. Li, T. Kottos, A. Alù, *Phys. Rev. Lett.* **2019**, *123*, 213901.
[38] K. Bai, L. Fang, T. R. Liu, J. Z. Li, D. Wan, M. Xiao, *Natl. Sci. Rev.* **2023**, *10*, nwac259.

 